THERMAL STRESS ANALYSIS OF LAMINATED PLATES USING GLOBAL-LOCAL HIGHER-ORDER MODEL

S.H. Lo[1], Wu Zhen[2] and Siu-Lai Chan[3]
1 Department of Civil Engineering, University of Hong Kong, Hong Kong, China. hreclsh@hku.hk
2 State Key Laboratory for Structural Analysis of Industrial Equipment, Dalian University of Technology, Dalian, China. wuzhenhk@163.com
3 Hong Kong Polytechnic University, Department of Civil & Environmental Engineering, Hong Kong, China. siu-lai.chan@polyu.edu.hk

ABSTRACT

A global-local higher order model taking into account transverse normal deformation is presented for the analysis of laminated composite plates subjected to the actual temperature field. The in-plane temperature field is expressed as a harmonic series expansion whereas the nonlinear temperature profile across the thickness direction is determined by solving the heat conduction equation. The validity of the proposed model is verified by comparing results with existing publications. Moreover, influence of the temperature fields along the thickness direction on the thermal behaviors of laminates is also investigated. A merit of the present model is that transverse shear stresses can be evaluated directly from the constitutive equations without stress smoothing.

KEYWORDS

Global-local higher order model, laminated composite plates, actual temperature fields, finite elements.

INTRODUCTION

With the increased use of composite materials in thermal environments, the thermal stress analysis of laminated composite materials has aroused considerable interests. Thermal deformation and stress in laminates have been analyzed by using equivalent single-layer models (ESLMs) (Reddy and Hsu 1980, Kheider and Reddy 1991, Kant and Khare 1994, Rohwer *et al*. 2001, Cho and Oh 2003, Wu and Chen 2006), in which the unknown variables are independent of the number of layers. More ESLMs for thermomechanical problems of laminated plates can be found in the review articles by (Tauchert 1991), (Noor and Burton 1992) and (Argyris and Tenek 1997). In addition, (Cho *et al*. 1989) and (Murakami 1993) used layerwise models to predict thermal response of multilayered plates. Based on the Reissner mixed variational theorem (RMVT), (Carrera 2000) employed the mixed layerwise model to predict thermal stresses of multilayered plates. In the mixed layerwise model, the transverse stress fields and the displacement fields within each layer are independently assumed.

Most of the previous research was concerned with the constant and linear temperature fields through the thickness of laminates. (Carrera 2002) studied the influence of the temperature fields on the response of multilayered plates. Analytical and numerical results showed that the temperature fields obtained by solving the heat conduction equation and the assumed linear temperature fields lead to rather different stresses and displacements. Moreover, Carrera concluded that the advanced zig-zag models could not produce accurate thermal stresses for temperature fields derived from the heat conduction equation. On the other hand, (Robaldo 2006) used finite element method based on layerwise model to investigate the influence of temperature profile on thermal response of multilayered plates. Layerwise model is more accurate than ESLMs, however this model is computationally expensive with increasing number of layers because the number of unknown variables depends on the number of layers of the laminate. Moreover, this model is unable to satisfy the continuity condition of transverse shear stresses at interfaces. In this paper, the global-local higher order model is used to analyze thermal response of laminated plates under temperature fields derived from the differential heat conduction equation in the thickness direction as proposed by (Tungikar and Rao 1994). In the finite element implementation, by means of the quadrilateral element DKQ developed by (Batoz and Tahar 1982), C^1 continuity of transverse displacement at the element interfaces is enforced.

GLOBAL-LOCAL HIGHER-ORDER THEORY

In the present model, the initial displacement fields are written as follows:

$$
\begin{aligned}
u^k(x,y,z) &= u_G(x,y,z) + \bar{u}_L^k(x,y,z) + \hat{u}_L^k(x,y,z) \\
v^k(x,y,z) &= v_G(x,y,z) + \bar{v}_L^k(x,y,z) + \hat{v}_L^k(x,y,z) \\
w^k(x,y,z) &= w_G(x,y,z)
\end{aligned} \tag{1}
$$

where u_G, v_G and w_G present global components of displacement; $\bar{u}_L^k$ and $\bar{v}_L^k$ are local displacements up to order ζ_k^2; $\hat{u}_L^k$ and $\hat{v}_L^k$ are local displacement of order ζ_k^3 as shown in eqn (3); the superscript *k* represents the layer order of laminated plates. The global coordinates associated with the plate are x, y, z. The reference plane ($z=0$) is taken at the mid-surface of the laminate. The local coordinates for a layer are denoted by x, y, ζ_k where $\zeta_k \in [-1,1]$. The relations between global coordinates and local coordinates are depicted in Figure 1. The global-local higher order theory has been studied (Wu and Chen 2006) and conclusion has been drawn that the fifth-order global-local theory is adequate for the problems of multi-layered plates. Based on the fifth-order in-plane components, the global displacement components are written as follows

$$
\begin{aligned}
u_G(x,y,z) &= \sum_{i=0}^{5} z^i u_i(x,y) \\
v_G(x,y,z) &= \sum_{i=0}^{5} z^i v_i(x,y) \\
w_G(x,y,z) &= \sum_{i=0}^{2} z^i w_i(x,y)
\end{aligned} \tag{2}
$$

The local components can be written as

$$
\begin{aligned}
\bar{u}_L^k(x,y,z) &= \zeta_k u_1^k(x,y) + \zeta_k^2 u_2^k(x,y) \\
\bar{v}_L^k(x,y,z) &= \zeta_k v_1^k(x,y) + \zeta_k^2 v_2^k(x,y) \\
\hat{u}_L^k(x,y,z) &= \zeta_k^3 u_3^k(x,y) \\
\hat{v}_L^k(x,y,z) &= \zeta_k^3 v_3^k(x,y)
\end{aligned} \tag{3}
$$

where $\zeta_k = a_k z - b_k$; $a_k = \dfrac{2}{z_{k+1} - z_k}$; $b_k = \dfrac{z_{k+1} + z_k}{z_{k+1} - z_k}$

Displacement continuity conditions

There are *6n+15* unknown variables in the initial displacement fields. By enforcing the displacement continuity conditions, 4(*n*-1) unknown variables can be eliminated. The continuity conditions proposed by (Li and Liu 1997) can be written as

$$
\begin{aligned}
\bar{u}_L^k(x,y,z_k) &= \bar{u}_L^{k-1}(x,y,z_k) \\
\hat{u}_L^k(x,y,z_k) &= \hat{u}_L^{k-1}(x,y,z_k) \\
\bar{v}_L^k(x,y,z_k) &= \bar{v}_L^{k-1}(x,y,z_k) \\
\hat{v}_L^k(x,y,z_k) &= \hat{v}_L^{k-1}(x,y,z_k)
\end{aligned} \qquad \text{where } k = 2,3,4,\cdots n \tag{4}
$$

Transverse shear stress continuity conditions

By imposing the continuity conditions of transverse shear stresses at interfaces, *2(n-1)* unknown variables can be eliminated. The transverse shear stress continuity conditions are given by

$$
\begin{aligned}
\tau_{xz}^k(x,y,z_k^-) &= \tau_{xz}^{k-1}(x,y,z_{k-1}^+) \\
\tau_{yz}^k(x,y,z_k^-) &= \tau_{yz}^{k-1}(x,y,z_{k-1}^+)
\end{aligned} \tag{5}
$$

where z_k^+ *and* z_k^- are respectively the z-coordinates at the top and at the bottom of the k[th] ply.
Now the number of unknown variables is reduced to 21. Further enforcing the free conditions of the transverse shear stresses on the upper and the lower surfaces, the number of independent unknowns is reduced to 17. Thus, the final displacement fields for cross-ply laminated plates are

$$u^k(x,y,z)=u_0(x,y)+\Phi_1^k(z)u_1^1(x,y)+\sum_{i=1}^{5}\Phi_{i+1}^k(z)u_i(x,y)+\sum_{j=0}^{2}\Phi_{i+7}^k(z)w_{i,x}$$
$$v^k(x,y,z)=v_0(x,y)+\Psi_1^k(z)v_1^1(x,y)+\sum_{i=1}^{5}\Psi_{i+1}^k(z)v_i(x,y)+\sum_{j=0}^{2}\Psi_{i+7}^k(z)w_{i,y} \quad (6)$$
$$w^k(x,y,z)=\sum_{i=0}^{2}z^i w_i(x,y)$$

where detailed expression for Φ_i^k and Ψ_i^k are given in (Wu Zhen and Chen Wanji, 2009).

TEMPERATURE FIELD

The initial temperature field proposed by (Tungikar and Rao 1994) is given by

$$T(x,y,z)=f(z)\sin(m\pi x/a)\sin(n\pi y/b) \quad (7)$$

where m and n are the wave number on the two principle directions of the plate; a and b are length and width of the laminated plate, respectively.

$$f(z)=T_0e^{sz} \quad (8)$$

T_0 is a constant and s is an unknown parameter. The Fourier equation of heat conduction for homogeneous orthotropic is given by

$$K_1\frac{\partial^2T}{\partial^2x}+K_2\frac{\partial^2T}{\partial^2y}+K_3\frac{\partial^2T}{\partial^2z}=0 \quad (9)$$

where K_1, K_2, K_3 are the thermal conductivities in the x, y and z directions. Substituting equations (7) and (8) into equation (9), expressions for unknown parameter s is given by

$$s_{1,2}=\pm\sqrt{\frac{K_1(m\pi/a)^2+K_2(n\pi/b)^2}{K_3}} \quad (10)$$

Hence, the temperature field for the *k*th layer is given by

$$T^k(x,y,z)=\left(C_1^k\cosh s_1z+C_2^k\sinh s_2z\right)\sin(m\pi x/a)\sin(n\pi y/b) \quad (11)$$

The temperature field equation (11) can also be found in Tungikar and Rao's paper and Carrera's paper. Enforcing the continuity conditions of temperature and heat flux q_z at interfaces as well as temperature boundary conditions on the upper and lower surfaces, $2N$ constants C_1^k and C_2^k can be determined. Continuity conditions of the temperature and the heat flux along the thickness direction at interfaces are given by

$$T^k(x,y,z_k^-)=T^{k-1}(x,y,z_{k-1}^+) \quad (12)$$
$$q_z{}^k(x,y,z_k^-)=q_z{}^{k-1}(x,y,z_{k-1}^+) \qquad \text{where } k=2,3,4,\cdots n \quad (13)$$

The heat flux for the *k*th ply is given by

$$q_z^k=K_3^k\frac{\partial T^k}{\partial z} \quad (14)$$

THE FOUR-NODE QUADRILATERAL LAMINATED PLATE ELEMENT

The strain components in the higher-order shear deformation theory possess first and second derivatives of transverse displacement *w*, and C^0 and C^1 continuity transverse displacement functions are required.

Transverse displacement function w^c satisfying C^0 continuity condition

Firstly, the transverse displacement function *w* is given by

$$w=\sum_{i=1}^{4}N_iw_i+\sum_{j=5}^{8}N_jw_j \quad (15)$$

where N_i is the shape function of the 8-node serendipity element.

To obtain the 4-node quadrilateral element, w_j at the mid-node along the element boundary can be eliminated using the Hermite cubic polynomials. For instance, using parameters θ_{si} and w_i at nodes 1 and 2, the interpolation of displacement $\widetilde{w}_s$ can be written as

$$\widetilde{w}_s = \sum_{i=1}^{2} H_i w_i + \sum_{i=1}^{2} H_{\theta i} \theta_{si} \tag{16}$$

where

$$\begin{aligned} H_1 &= L_1 + L_1 L_2 (L_1 - L_2) \\ H_2 &= L_2 + L_1 L_2 (L_2 - L_1) \\ H_{\theta 1} &= (L_1 L_2 + L_1 L_2 (L_1 - L_2)) S_1 / 2 \\ H_{\theta 2} &= (-L_1 L_2 + L_1 L_2 (L_1 - L_2)) S_1 / 2 \end{aligned} \tag{17}$$

in which θ_{si} is the tangential slopes at the node i (i=1,2) on the boundary; S_1 is the length between nodes 1 and 2; $L_1 = 1 - \dfrac{S}{S_1}$ and $L_2 = \dfrac{S}{S_1}$ in which S is the coordinates along the 1-2 edge. Substituting $L_1 = L_2 = 0.5$ in equation (16), w_5 at the mid-node 5 on the 1-2 boundary is given by

$$w_5 = \frac{1}{8}\left(4w_1 + S_1\theta_{s1} + 4w_2 - S_1\theta_{s2}\right) \tag{18}$$

where θ_{sj} ($j = 1,2,5$) on 1-2 boundary are given by

$$\theta_{sj} = \begin{bmatrix} -m_1 & \ell_1 \end{bmatrix} \begin{Bmatrix} \theta_{xj} \\ \theta_{yj} \end{Bmatrix} \quad (j=1,2,5) \tag{19}$$

where l, m are the direction cosines normal to the boundary. Substituting equation (19) in equation (18), the following equation for w_5 can be obtained

$$w_5 = \frac{1}{8}\begin{bmatrix} 4 & -m_1 S_1 & \ell_1 S_1 & 4 & m_1 S_1 & -\ell_1 S_1 \end{bmatrix} \begin{Bmatrix} w_1 \\ \theta_{x1} \\ \theta_{y1} \\ w_2 \\ \theta_{x2} \\ \theta_{y2} \end{Bmatrix} \tag{20}$$

Similarly other mid-node parameters w_j ($j = 6,7,8$) are expressed by nodal parameters $[w_j \quad \theta_{xj} \quad \theta_{yj}]^T$ ($j = 1 \sim 4$). Substituting mid-node parameters w_j ($j = 5 \sim 8$) into equation (15), finally, an explicit expression for the C^0 continuity displacement function can be written as follows

$$w^c = Fq \tag{21}$$

where $F = \begin{bmatrix} F_i & F_{xi} & F_{yi} \end{bmatrix}$, $q = \left\{ w_i, w_{xi}, w_{yi} \right\}^T$ and

$$\begin{aligned} F_1 &= 0.5(m_1 N_5 / S_1 - m_4 N_8 / S_4) + N_1^{\oplus} \\ F_{x1} &= -0.125(m_1^2 N_5 + m_4^2 N_8) \\ F_{y1} &= 0.125(\ell_1 m_1 N_5 + \ell_4 m_4 N_8) \\ N_i^{\oplus} &= \frac{1}{4}(1 + \xi\xi_i)(1 + \eta\eta_i), \; i = 1,2,3,4. \end{aligned} \tag{22}$$

Other shape functions, namely, $\begin{bmatrix} F_i & F_{xi} & F_{yi} \end{bmatrix} (i = 2,3,4)$ can be obtained by cyclic permutation.

Transverse displacement function w^* satisfying C^1 continuity condition

To obtain the transverse displacement function w^* satisfying C^1 continuity condition, the rotation function of the thin plate quadrilateral element DKQ (Batos and Tahar 1982) is adopted as C^1-continuity requirement is satisfied at the inter-element boundaries in strict sense and continuity condition in the element in an average sense (Chen and Cheung 1997). The explicit expressions for rotations of element DKQ are given by

$$\begin{Bmatrix} \theta_x \\ \theta_y \end{Bmatrix} = \overline{N} q \tag{23}$$

where

$$\overline{\boldsymbol{N}} = \begin{bmatrix} \overline{\boldsymbol{N}}_1 & \overline{\boldsymbol{N}}_2 & \overline{\boldsymbol{N}}_3 & \overline{\boldsymbol{N}}_4 \end{bmatrix} \tag{24}$$

$$\overline{\boldsymbol{N}}_j = \begin{bmatrix} P_j & P_{xj} & P_{yj} \\ Q_j & Q_{xj} & Q_{yj} \end{bmatrix}, \quad (j = 1,2,3,4) \tag{25}$$

$$\begin{aligned} P_1 &= 1.5(m_1 N_5 / S_1 - m_4 N_8 / S_4) \\ P_{x1} &= -0.75(m_1^2 N_5 + m_4^2 N_8) + N_1^{\oplus} \\ P_{y1} &= 0.75(\ell_1 m_1 N_5 + \ell_4 m_4 N_8) \\ Q_1 &= 1.5(-\ell_1 N_5 / S_1 + \ell_4 N_8 / S_4) \\ Q_{x1} &= 0.75(\ell_1 m_1 N_5 + \ell_4 m_4 N_8) \\ Q_{y1} &= -0.75(\ell_1^2 N_5 + \ell_4^2 N_8) + N_1^{\oplus} \end{aligned} \tag{26}$$

with

$$\ell_1 = \frac{y_{21}}{\sqrt{x_{12}^2 + y_{21}^2}};\ m_1 = \frac{x_{12}}{\sqrt{x_{12}^2 + y_{21}^2}};\ \ell_4 = \frac{y_{14}}{\sqrt{x_{41}^2 + y_{14}^2}};\ m_4 = \frac{x_{41}}{\sqrt{x_{41}^2 + y_{14}^2}}$$

$$y_{21} = y_2 - y_1;\ x_{12} = x_1 - x_2;\ y_{14} = y_1 - y_4;\ x_{41} = x_4 - x_1$$

Using the rotations function of DKQ element, the second derivatives of transverse displacement function w^* satisfying C^1 continuity condition is given by

$$\begin{aligned} \frac{\partial^2 w^*}{\partial x^2} &= \frac{\partial \theta_x}{\partial x} \\ \frac{\partial^2 w^*}{\partial y^2} &= \frac{\partial \theta_y}{\partial y} \\ \frac{\partial^2 w^*}{\partial x \partial y} &= \frac{1}{2}\left(\frac{\partial \theta_y}{\partial x} + \frac{\partial \theta_x}{\partial y} \right) \end{aligned} \tag{27}$$

Displacement functions

In terms of nodal variables and shape functions, primary displacement unknowns can be expressed as follows

$$\begin{aligned} \overline{U} &= \sum_{i=1}^{4} N_i^{\oplus} \overline{U}_i \\ w^c &= \sum_{i=1}^{4} (F_i w_{0,i} + F_{xi} w_{0,xi} + F_{yi} w_{0,yi}) \\ w^* &= \sum_{i=1}^{4} (F_i^* w_{0,i} + F_{xi}^* w_{0,xi} + F_{yi}^* w_{0,yi}) \end{aligned} \tag{28}$$

where $\overline{U} = \begin{bmatrix} u_0 & v_0 & u_1^1 & u_1 & u_2 & u_3 & u_4 & u_5 & v_1^1 & v_1 & v_2 & v_3 & v_4 & v_5 \end{bmatrix}$.

Strain matrix and stiffness matrix

According to linear strain-displacement relations, the strain for the kth layer can be written as follows:

$$\varepsilon^k = \partial u^k = \begin{bmatrix} B_1 & B_2 & B_3 & B_4 \end{bmatrix} \delta^e \tag{29}$$

where $\delta^e = [\delta_1^e \quad \delta_2^e \quad \delta_3^e \quad \delta_4^e]^T$, and for i = 1, 2, 3, 4

$$\delta_i^e = \begin{bmatrix} u_{0i} & v_{0i} & w_{0i} & w_{1i} & w_{2i} & u_{1i}^1 & u_{1i} & \cdots & u_{5i} & w_{0xi} & w_{1xi} & w_{2xi} & v_{1i}^1 & v_{1i} & \cdots & v_{5i} & w_{0yi} & w_{1yi} & w_{2yi} \end{bmatrix}$$

$$[\partial] = \begin{bmatrix} \frac{\partial}{\partial x} & 0 & 0 & \frac{\partial}{\partial z} & 0 & \frac{\partial}{\partial y} \\ 0 & \frac{\partial}{\partial y} & 0 & 0 & \frac{\partial}{\partial z} & \frac{\partial}{\partial x} \\ 0 & 0 & \frac{\partial}{\partial z} & \frac{\partial}{\partial x} & \frac{\partial}{\partial y} & 0 \end{bmatrix}^T$$

The detailed expression of the strain matrix can be obtained by the method proposed by (Wu et al. 2005, 2014). From strain matrix *B* of the refined nonconforming element, the element stiffness matrix K^e is given by

$$\left[K^e\right] = \sum_{i=1}^{n} \int_{i-1}^{i} \left(\iint B^T Q_i B dx dy \right) dz \tag{30}$$

On solving the global stiffness equation, nodal displacement $\left\{\delta^e\right\}$ for load vector $\{r\}$ can be obtained

$$\sum \left[K^e\right]\left\{\delta^e\right\} = \{r\} \tag{31}$$

NUMERICAL EXAMPLES

To assess the performance of the proposed model for laminates under actual temperature field, two examples are presented. Owing to symmetry, only one-quarter of the laminated plate has been modeled. The plate geometry and a 4×4 mesh configuration are shown in Figure 2. The following publications are referred to for comparison.

(Robaldo 2006) - T_1: Layerwise finite element results according to actual temperature profile through the thickness direction.

(Robaldo 2006) - T_2 : Layerwise finite element results according to the assumed temperature profile.

(Kapuria and Achary 2004) Exact thermo-elasticity solution.

HZIGT (Kapuria and Achary 2004) Analytical results based on higher order zig-zag model including transverse normal deformation. Transverse shear stresses are calculated using the 3D equilibrium equations.

ZIGT (Kapuria and Achary 2004) Analytical results based on higher order zig-zag model neglecting transverse normal deformation. Transverse shear stresses are calculated using the 3D equilibrium equations.

Example 1. Simply-supported 3-ply square plate $(0^\circ/90^\circ/0^\circ)$ subjected to actual temperature field $T_1(z)\sin\frac{\pi x}{a}\sin\frac{\pi y}{b}$ and assumed temperature field $T_2(z)\sin\frac{\pi x}{a}\sin\frac{\pi y}{b}$. Actual temperature profile through the thickness direction $T_1(z)$ can be obtained by solving heat conduction equation as discussed in the section of TEMPERATURE FIELD. Temperatures at the top and bottom surfaces are $T_t = 1$ and $T_b = -1$, respectively. Linear through-the-thickness temperature profile $T_2(z)$ is assumed as $T_2(z) = T_0 \frac{2z}{h}$ where $T_0 = 1$. Distributions of two temperature profiles along the thickness direction can be found in Figure 3. The material constants are given as follows

$$E_L / E_T = 25,\ G_{LT} / E_T = 0.5,\ G_{TT} / E_T = 0.2,\ v_{LT} = v_{TT} = 0.25$$

$$\alpha_T / \alpha_L = 1125,\quad K_L = 36W/m^\circ C,\ K_T = 0.96W/m^\circ C$$

where *L* and *T* respectively represent directions parallel and perpendicular to the fibers. The displacements and stresses are normalized by

$$\bar{u}(a/2,0,z) = \frac{u(a/2,0,z)}{a\alpha_L};\ \bar{\tau}_{yz}(0,b/2,z) = \frac{\bar{\tau}_{yz}(0,b/2,z)}{E_T\alpha_L}$$

In-plane displacements for both the assumed and the actual temperature fields are compared with results of layerwise model in Figure 4. It is found that the present results agree well with those of layerwise model. Moreover, the difference of in-plane displacements between the actual temperature field and the assumed temperature field is quite noticeable. Furthermore, the influence of temperature profile on the transverse shear stress can be seen in Figure 5.

Example 2. Simply-supported 3-ply square plate ($0^o/90^o/0^o$) subjected to specified temperature fields $T_3(z)\sin\frac{\pi x}{a}\sin\frac{\pi y}{b}$ and $T_4(z)\sin\frac{\pi x}{a}\sin\frac{\pi y}{b}$. For temperature profile $T_3(z)$, temperatures at the top and bottom surfaces are defined as $T_t=1$ and $T_b=1$. However, temperatures at the top and bottom surfaces for $T_4(z)$ are $T_t=1$ and $T_b=-1$, respectively. Temperature fields $T_3(z)$ and $T_4(z)$ are shown in Figures 6 and 7. The material constants used are given as follows

$$E_L=181GPa,\ E_T=10.3GPa,\ G_{LT}=7.17GPa,\ G_{TT}=2.87GPa,\ v_{LT}=0.28,\ v_{TT}=0.33$$

$$\alpha_L=0.02\times10^{-6}/K,\ \alpha_T=22.5\times10^{-6}/K,\ K_L=1.5W/mK,\ K_T=0.5W/mK$$

The displacements and stresses are normalized by

$$\bar{u}(a/2,0,z)=\frac{100u(a/2,0,z)}{a\alpha_T T_0},\ \bar{v}(0,b/2,z)=\frac{100v(0,b/2,z)}{a\alpha_T T_0},\ \bar{w}(0,0,z)=\frac{100w(0,0,z)h}{a^2\alpha_T T_0},$$

$$\bar{\sigma}_x(0,0,z)=\frac{\sigma_x(0,0,z)}{\alpha_T E_T T_0},\ \bar{\sigma}_y(0,0,z)=\frac{\sigma_y(0,0,z)}{\alpha_T E_T T_0},\ \bar{\tau}_{xz}(a/2,0,z)=\frac{\tau_{xz}(a/2,0,z)L}{\alpha_T E_T T_0 h},$$

$$\bar{\tau}_{yz}(0,b/2,z)=\frac{\tau_{yz}(0,b/2,z)L}{\alpha_T E_T T_0 h},\ T_0=1$$

Distributions of through-the-thickness displacements and stresses for plates under temperature profile $T_3(z)$ obtained from the present model are compared with the exact thermo-elasticity solutions and the existing zig-zag models (HZIGT and ZIGT) in Figures 8-11. It is found that the present results agree well with exact solutions whereas higher order zig-zag model (HZIGT) as well as ZIGT seems less accurate. Moreover, transverse shear stresses $\bar{\tau}_{xz}$ computed directly from constitutive equations are also in good agreement with the exact solutions. Results for displacements and stresses of laminated plates subjected to temperature profile $T_4(z)$ are presented in Figures 12-14.

CONCLUSIONS

Thermal response of laminated composite plates under actual temperature field has been studied by using the global-local higher-order theory. The results are compared with exact solutions and those previously published. From the comparison, the following conclusions can be drawn:

1. When the actual temperature field through the thickness direction differs significantly from the assumed temperature field over a thick plate, the two temperature profiles do lead to very different thermal response.
2. Higher-order zig-zag model neglecting transverse normal deformation is not adequate for the thermal problems of laminated plates subjected to general temperature fields.
3. Compared with higher-order zig-zag models, the present model usually gives more accurate results for the thermal response of laminated plate. For a laminated plate with different thickness and materials at each ply, the transverse shear stress can be determined directly from the constitutive equations.

ACKNOWLEDGEMENTS

The URC/CRCG – Conference Support for Teaching Staff of the University of Hong Kong is gratefully acknowledged.

REFERENCES

Argyris J and Tanek L (1997) "Recent advances in computational thermostructural analysis of composite plates and shells with strong nonlinearities", *Appl Mech Rev*., **50**, 285-306.

Batoz JL and Tahar M.B. (1982). "Evaluation of a new quadrilateral thin plate bending element", *Int. J. Numer. Meth Eng*., **18**, 1655-1677.

Carrera E (2000). "An assessment of mixed and classical theories for the thermal stress analysis of orthotropic multilayered plates", *J Thermal Stresses*, **23**, 797-831.

Carrera E (2002). "Temperature profile influence on layered plates response considering classical and advanced theories", *AIAA J*., 40(9), 1885-1896.

Chen Wanji and Cheung Y.K. (1997). "Refined quadrilateral discrete Kirchhoff thin plate bending element", *Int. J. Numer. Methods Eng.*, **40**, 3937-3953.
Cho KN, Bert CW and Striz AG (1989). "Thermal stress analysis of laminate using higher order individual-layer theory", *J Thermal Stresses*, **12**, 321-332.
Cho M and Oh J (2003). "Higher order zig-zag plate theory under thermo-electric-mechanical loads combined", *Composites: Part B*, **34**, 67-82.
Kant T and Khare RK (1994). "Finite element thermal stress analysis of composite laminates using a higher order theory", *J Thermal Stresses*, **17**, 229-255.
Kapuria S and Achary GGS (2004). "An efficient higher order zigzag theory for laminated plates subjected to thermal loading", *Int J Solids Struct.*, **41**, 4661-4684.
Kapuria S, Dumir PC and Ahmed A (2003). "An efficient higher order zigzag theory for composite and sandwich beams subjected to thermal loading", *Int J Solids Struct.*, **40**, 6613-6631.
Kheider AA and Reddy JN (1991). "Thermal stresses and deflections of cross-ply laminated plates using refined theories", *J Thermal Stresses*, **14**, 419-438.
Li XY and Liu. D. (1997). "Generalized laminate theories based on double superposition hypothesis", *Int. J. Numer. Methods Eng.*, **40**, 1197-1212.
Noor AK and Burton WS (1992). "Computational models for high-temperature multilayered composite plates and shells", *Appl Mech Rev.*, 45(10), 419-446.
Murakami H (1993). "Assessment of plate theories for treating the thermomechanical response of layered plates", *Compos Engrg.*, 3(2), 137-149.
Reddy JN and Hsu YS (1980). "Effects of shear deformation and anisotropy on the thermal bending of layered composite plates", *J Thermal Stresses*, **3**, 475-493.
Robaldo A (2006). "Finite element analysis of the influence of temperature profile on thermoelasticity of multilayered plates", *Comput Struct.*, **84**, 1236-1246.
Rohwer K, Rolfes R and Sparr H (2001). "Higher order theories for thermal stresses in layered plates", *Int J Solids Struct.*, **38**, 3673-3687.
Tauchert TR (1991). "Thermally induced flexure, buckling and vibration of plates", *Appl Mech Rev.*, 44(8), 347-360.
Tungikar VB and Rao KM (1994). "Three dimensional exact solution of thermal stresses in rectangular composite laminates", *Compos Struct.*, **27**, 419-427.
Wu Zhen, Chen Ronggeng and Chen Wanji (2005). "Refined laminated composite plate element based on global-local higher-order shear deformation theory", *Compos Struct.*, **70**, 135-152.
Wu Zhen and Chen Wanji (2006). "An efficient higher-order theory and finite element for laminated plates subjected to thermal loading", *Compos Struct.*, **73**, 99-109.
Wu Zhen and Chen Wanji (2007). "Refined global-local higher-order theory and finite element for laminated plates", *Int. J. Numer. Meth Eng.*, 69(8), 1627-1670.
Wu Zhen and Chen Wanji (2009). "A higher-order displacement model for stress concentration problems in general lamination configurations", *Material & Design*, 30(5), 1458-1467.

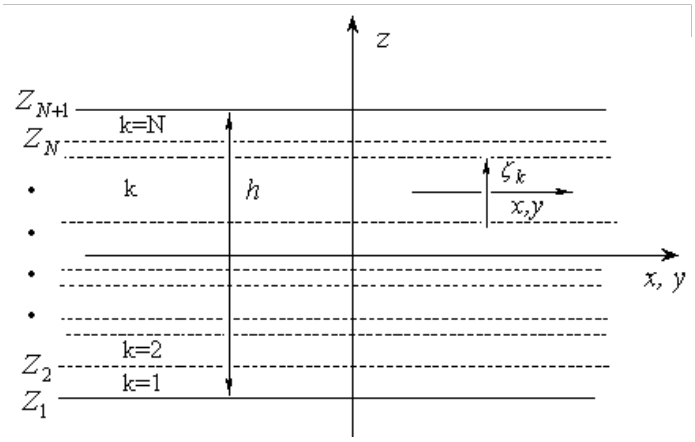

Fig. 1 Schematic diagram for laminated plate segment

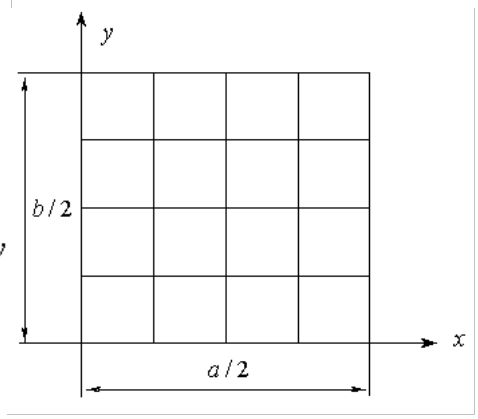

Fig. 2 A quarter of the plate divide into a 4×4 mesh

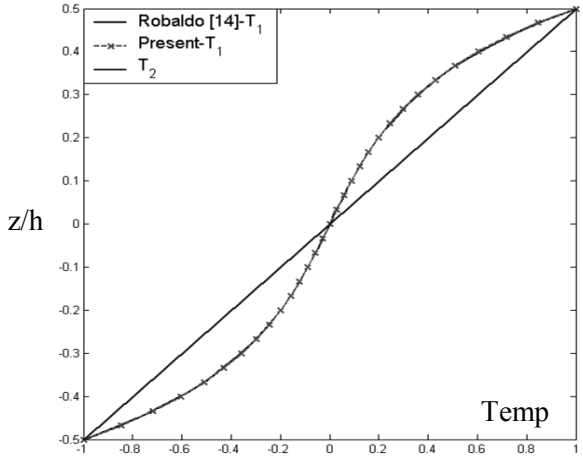

Fig. 3 Actual temperature field and assumed temperature field (*a*/*h*=4)

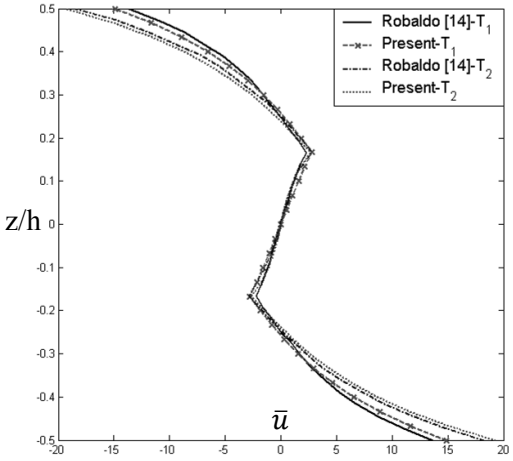

Fig. 4 In-plane displacement of layerwise models and the present model (*a*/*h*=4)

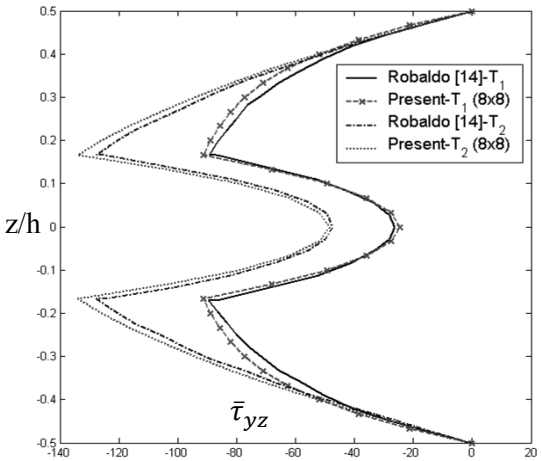

Fig. 5 Transverse shear stress of layerwise model and the present model (*a*/*h*=4)

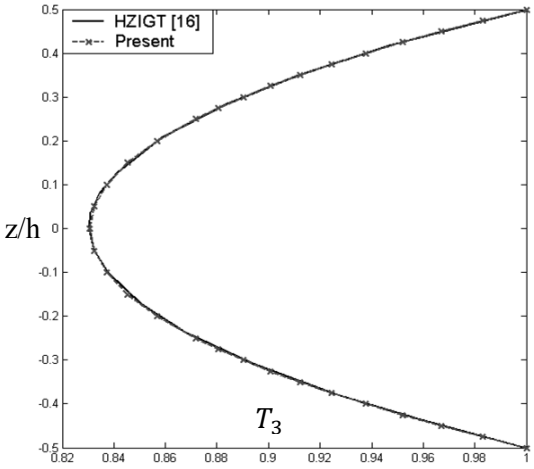

Fig. 6 Temperature distribution (T_3) through thickness of laminates (*a*/*h*=5)

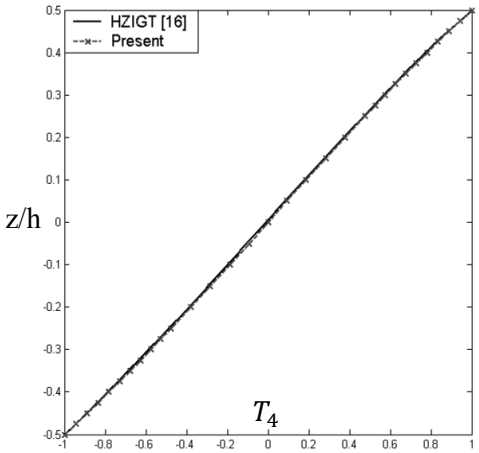

Fig. 7 Temperature distribution (T_4) through thickness of laminates (*a*/*h*=5)

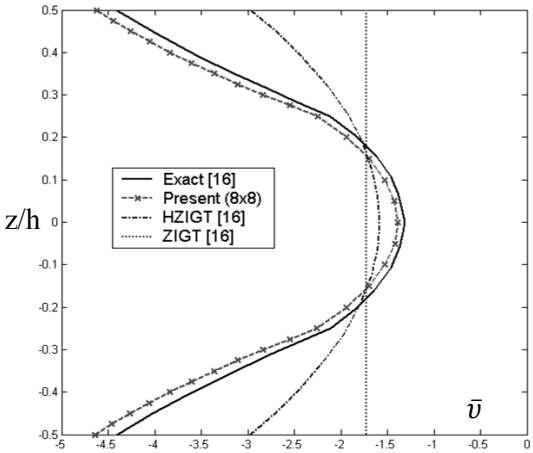

Fig. 8 In-plane displacement ($\bar{v}$) of different models (*a*/*h*=5)

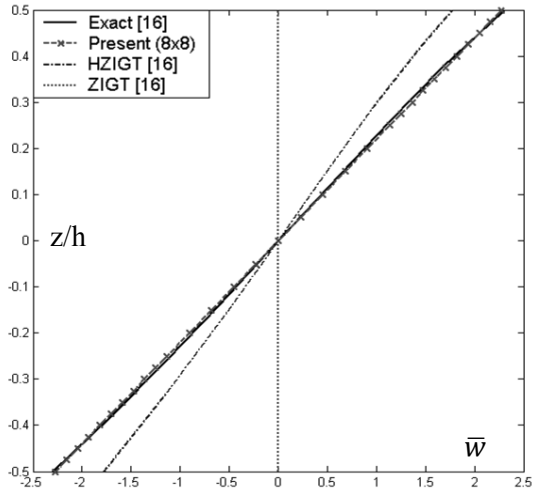

Fig. 9 Transverse displacement ($\bar{w}$) of different models (a/h=5)

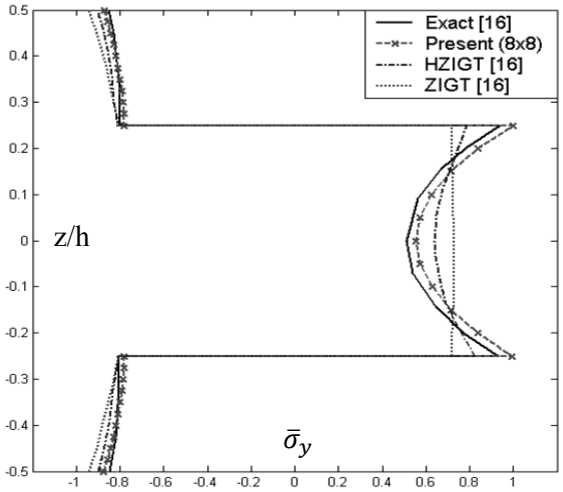

Fig. 10 In-plane stresses ($\bar{\sigma}_y$) of different models (a/h=5)

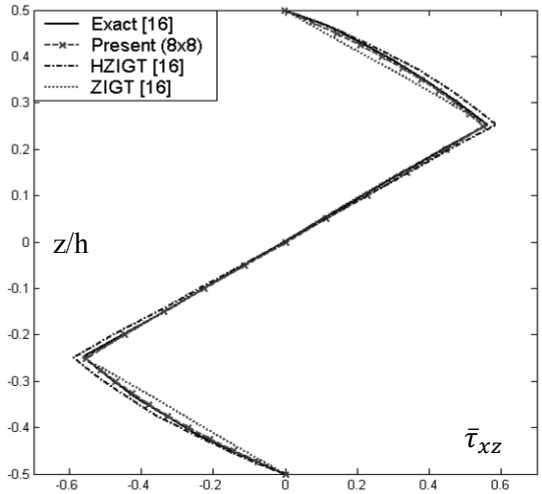

Fig. 11 Transverse shear stress ($\bar{\tau}_{xz}$) of different models (a/h=5)

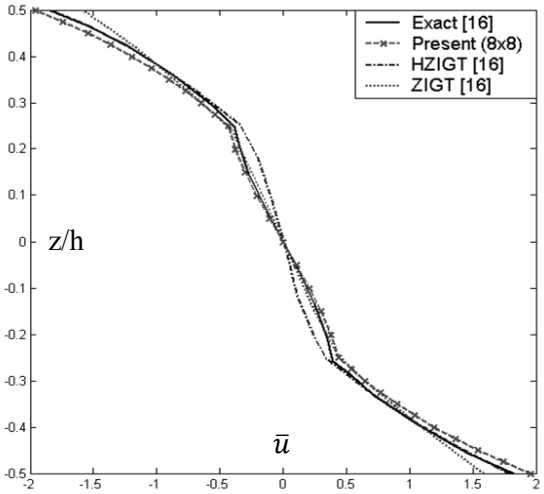

Fig. 12 In-plane displacement ($\bar{u}$) of different models (a/h=5)

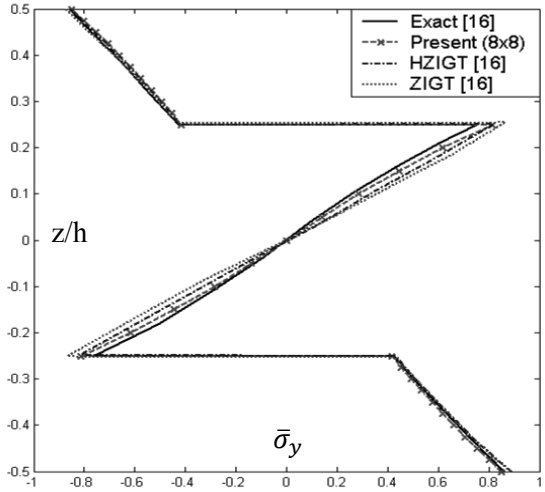

Fig. 13 In-plane stresses of different models (a/h=5)

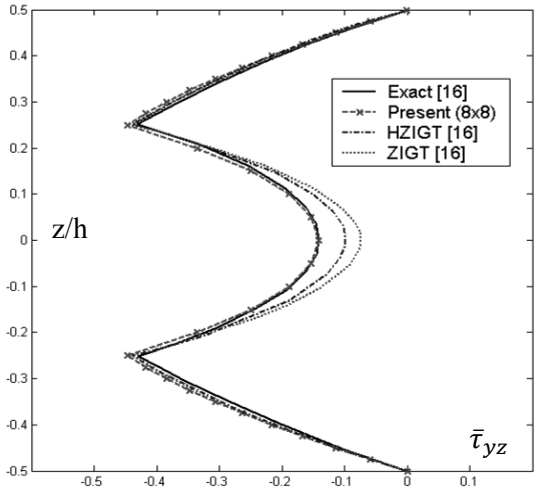

Fig. 14 Transverse shear stresses of different models (a/h=5)